Nano Select

RESEARCH ARTICLE OPEN ACCESS

Curcumins-Loaded ZIF-8 Nanoparticles-Embedded Transdermal Polymeric Patches Increase Apoptosis and Reduce Necrosis in a Dose-Dependent Manner in MCF-7 Cells

Humeysa Kiyak-Kirmaci[1] | Saliha Aydin[2,3,4] | Humeyra Betul Yekeler[2,5,6] | Ece Guler[5,6,7] | Ayse Beyza Kayaci[2] | Zeynep Gurer[2] | Ayse Mine Yilmaz-Goler[3,8] | Ziya Engin Erkmen[9] | Ozgur Duygulu[10] | Muge Sennaroglu Bostan[11] | Diana Martins[12,13,14,15] | Fernando Mendes[12,13,14,15,16] | Mehmet Sayip Eroglu[6,10,11] | Mohan Edirisinghe[17] | Muhammet Emin Cam[3,5,6,7,17,18]

[1]Department of Pharmacology, Hamidiye Faculty of Pharmacy, University of Health Sciences, Istanbul, Türkiye | [2]Department of Pharmacology, Faculty of Pharmacy, Marmara University, Istanbul, Türkiye | [3]Genetic and Metabolic Diseases Research and Investigation Center, Marmara University, Istanbul, Türkiye | [4]Dr. Siyami Ersek Thoracic and Cardiovascular Surgery Education Research School, Istanbul, Türkiye | [5]MecNano Technologies, Cube Incubation, Teknopark Istanbul, Istanbul, Türkiye | [6]Center for Nanotechnology and Biomaterials Application and Research, Marmara University, Istanbul, Türkiye | [7]Department of Pharmacology, Faculty of Pharmacy, Istanbul Kent University, Istanbul, Türkiye | [8]Department of Biochemistry, Faculty of Medicine, Marmara University, Istanbul, Türkiye | [9]Department of Metallurgical and Materials Engineering, Faculty of Engineering, Marmara University, Istanbul, Turkey | [10]TUBITAK Marmara Research Center, Materials Institute, Gebze, Kocaeli, Turkey | [11]Department of Chemical Engineering, Faculty of Engineering, Marmara University, Istanbul, Turkey | [12]Polytechnic University of Coimbra, Coimbra, Portugal | [13]H&TRC-Health & Technology Research Center, Coimbra Health School, Polytechnic University of Coimbra, Coimbra, Portugal | [14]Biophysics Institute of Faculty of Medicine, Coimbra Institute for Clinical and Biomedical Research (iCBR) Area of Environment Genetics and Oncobiology (CIMAGO), University of Coimbra, Coimbra, Portugal | [15]Center for Innovative Biomedicine and Biotechnology, University of Coimbra, Coimbra, Portugal | [16]European Association of Biomedical Scientists, Brussels, Belgium | [17]Department of Mechanical Engineering, University College London, London, UK | [18]Biomedical Engineering Department, University of Aveiro, Aveiro, Portugal

Correspondence: Mehmet Sayip Eroglu (mehmet.eroglu@marmara.edu.tr) | Mohan Edirisinghe (m.edirisinghe@ucl.ac.uk) | Muhammet Emin Cam (muhammet.cam@kent.edu.tr)

Received: 14 May 2025 | **Revised:** 15 July 2025 | **Accepted:** 21 July 2025

Funding: This project was supported by a TUBITAK 2209-A Research Projects Program Grant (2209-A, 2022/-1, No: 1919B012208840, Scientific and Technological Research Council of Turkey-TUBITAK).

Keywords: cancer | curcumin | ZIF-8 nanoparticle

ABSTRACT

Curcumin(Cur)-loaded zeolitic imidazolate framework-8 (ZIF-8) nanoparticles (Cur@ZIF-8 NPs) were produced to increase the anticancer activity of Cur. Cur@ZIF-8 NPs were embedded in polycaprolactone (PCL) fibers as transdermal polymeric patches via a pressured gyration (PG) method to provide controlled release. Cur@ZIF-8 NPs and Cur@ZIF-8 NPs-embedded PCL fibers were characterized for physical, chemical, mechanical, and thermal properties, also biological activities were examined with in vitro tests. Cur@ZIF-8 NPs were produced homogeneously with a size of ~200 nm and a zeta potential of ~−19 mV. Cur had better stability inside Cur@ZIF-8 NPs than its powder form. Cur@ZIF-8 NPs were successfully loaded in PCL fibers with a size of ~7 µm, and Cur@ZIF-8 NPs were dispersed amorphously in fibers. Cur was released in a controlled manner, and its efficiency was increased in the acidic microenvironment that is characteristic of cancer. Cur@ZIF-8 NPs have more bioavailability than powdered Cur and can penetrate the cells to deliver their anticancer effects on MCF-7 human breast cancer cells. Cur@ZIF-8 NPs-embedded

transdermal polymeric patches promote apoptosis in MCF-7 cells by reducing necrosis, particularly under acidic conditions. This work presents a release system with synergistic anticancer effects, offering a novel approach for Cur's clinical application in breast cancer through enhanced targeting.

1 | Introduction

Cancer is rated as the leading cause of death and the greatest obstacle to life expectancy in the 21st century [1]. Considering adjusted cancer cell metabolism, solid tumors create, and excrete excessive amounts of lactic acid. Since it is associated with inadequate vascular perfusion, an acidic microenvironment develops in the extracellular space [2]. One type of cancer that manifests commonly in women is breast cancer (BC), which ranks first with respect to cancer deaths [3]. Surgery, radiotherapy, and chemotherapy are frequently used in combination as current BC treatment options. Even though commonly used techniques such as surgery, radiotherapy, and chemotherapy slow the progression of cancer, their cytotoxic side effects cause disproportionate harm to healthy cells. Less toxic and non-resistant novel anticancer therapy is of utmost importance to overcome the drawbacks of existing BC treatment alternatives [4].

Curcumin (Cur) is a polyphenolic natural product isolated from the rhizomes of *Curcuma longa*. Owing to Cur's anticancer, anticoagulant, antibacterial, and anti-inflammatory properties; it has had a significant impact as a promising bioactive compound [5, 6]. Cur is beneficial for numerous diseases along with certain types of cancers. Cur has the ability to downregulate nuclear factor-kappa B (NF-κB) induced genes, thereby affecting the proliferation and invasion of BC cells. NF-κB pathway, a transcription factor that promotes inflammation, is activated in BC cells. Inhibition of the NF- κB pathway is one of the possible routes for BC treatment [7, 8]. Cur exhibits poor pharmacokinetic features, including limited intestinal absorption, low bioavailability, fast rate of metabolism, and short half-life elimination, while having anticancer potential. Thus, nanotechnology can faster a novel approach to refine its insufficient pharmacokinetic features [9].

Nanotechnology presents an exciting prospect in the field of biomedical research by leveraging nanomaterials and nanoscale particles for diagnosis, imaging, and treatment in nanomedical practices [10, 11]. The advancement of novel applications to drug delivery systems (DDSs) has transformed into a new perspective instrument in the pharmaceutical industry in tandem with the emergence of nanotechnology [12, 13]. The most significant benefits of DDSs comprise controllable pharmacokinetics and bioavailability of an active ingredient for different purposes. Advanced DDSs like fibers, particles, microspheres, nanogels, and micelles tend to increase efficacy and patient compliance and diminish adverse effects [12, 14].

Metal-organic frameworks (MOFs), which are used in drug delivery, materials science, biomedical, and chemistry applications, are new and remarkable structures [15, 16]. Because of their distinguishing qualities such as tunable pore sizes, wide surface areas, easy surface modification, high thermal stability, supplying controlled release, and enhancement of bioavailability of pharmaceutical active ingredients MOFs are preferred in DDSs [17, 18]. Recently, nano-sized MOFs have been designed to respond to chemical or physical stimuli. Therefore MOFs show promising results for cancer therapy [17].

Zeolitic imidazole frameworks (ZIFs), which have been frequently used in nanotechnology in recent years due to their adaptability and beneficial properties, are subspecies of MOFs that demonstrate exceptional morphological properties [17]. ZIFs have wide surfaces and high porosities which increase their loading capacity. In addition, their outstanding thermal stability and distinctive topologies make ZIFs more attractive structures [18].

ZIF-8 is composed of 2-methylimidazole and Zn^{2+} ions. ZIF-8 has been used in controlled drug release systems in recent years [15]. ZIF-8, which is often preferred due to its simple synthesis methods and its reasonable cost can be achieved by modifying the experimental conditions [19]. Also, under specific experimental conditions, ZIF-8 has low toxicity [20]. Additionally, ZIF-8 has excellent adsorption capacity, biocompatibility, and pH-responsiveness [18]. ZIF-8 shows high stability in physiological conditions and dissociates under acidic conditions. ZIF-8 is a very attractive candidate for the new generation of pH-sensitive DDSs through its capability of separation under acidic conditions. Cancer cells have an acidic microenvironment because of their changing metabolism [17]. It has been shown that the acidic microenvironment can be used in targeted therapy due to the possibilities of nanotechnology in the last decades [21]. ZIF-8 is regarded as one of the best candidates for targeted cancer therapy since it can be better disintegrated at acidic pH and thereby successfully release drugs [22].

Fibers have unique properties such as high porosity, high mechanical strength, and a large surface area [23]. In recent years DDSs have been incorporated in cancer therapy using fibers [12, 24]. Fibers are produced by using polymers, such as PCL, which is an FDA-approved polymer with a slow degradation rate and extremely good solubility [25]. PCL, a hydrophobic polymer, has excellent biocompatibility and biodegradability and is often preferred in DDSs due to its high drug permeability [26–28]. Furthermore, one of the most significant advantages of PCL is its minimal immunological response [29]. Moreover, PCL fibers can be used in transdermal applications with their high mechanical strength and controlled release features [27]. PCL degrades slowly, and therefore, it is ideal for tissue engineering and sustained release medication delivery systems for cancer treatment [30]. For instance, Chen et al. produced PCL fibers loaded with doxorubicin, Cur, and magnetic nanoparticles (NPs) for breast cancer treatment. PCL fibers ensured continuous release of drugs for up to 2 months, eliminating the burden of repeated applications on patients. The results showed that fiber-mediated administration of anti-cancer agents was beneficial

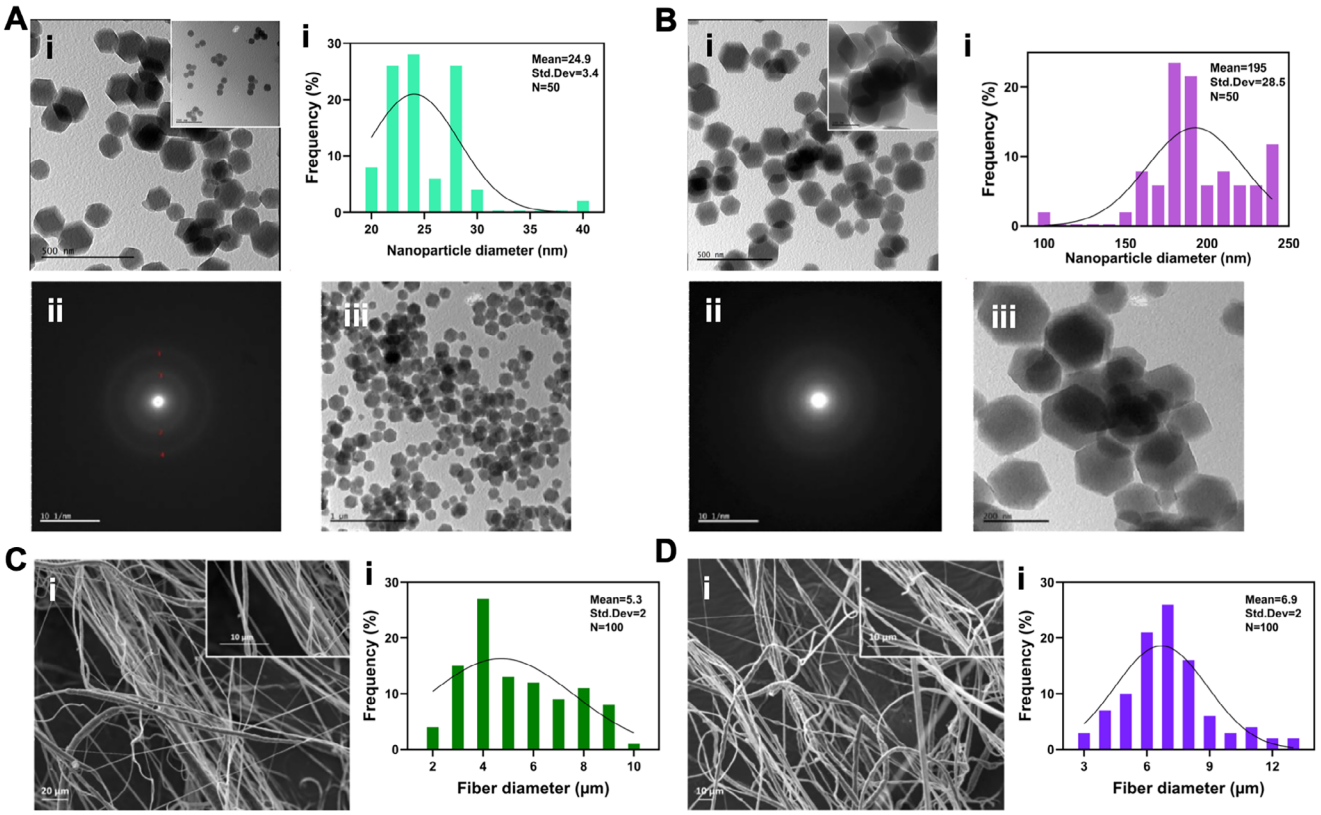

FIGURE 1 | Structures and morphological analyses. (A) (i) TEM images and nanoparticle diameters of pure zeolitic imidazolate framework-8 nanoparticle (pure ZIF-8 NP), (ii) SAED patterns of pure ZIF-8 NPs, (iii) TEM images of pure ZIF-8 NP. (B) (i) TEM images and nanoparticle diameters of curcumin-loaded zeolitic imidazolate framework-8 nanoparticle (Cur@ZIF-8 NP), (ii) SAED patterns of Cur@ZIF-8 NP, (iii) TEM images of Cur@ZIF-8 NP. (C) (i) SEM images and fiber diameters of virgin PCL fibers. D. (i) SEM images and fiber diameters of Cur@ZIF-8 NP-embedded PCL fiber.

in patients who had undergone breast-conserving surgery or mastectomy [31]. Additionally, Sridhar et al. produced PCL fibers containing curcumin, aloe vera, and neem extracts and evaluated their in vitro anti-cancer activity in MCF-7 and A459 cell lines. The results showed that curcumin and aloe vera-loaded fibers had 15 times higher cytotoxicity than the control group in both cell lines [32]. Due to all these properties of PCL and the successful results obtained with PCL fibers in the literature, fibers were produced using PCL polymer in our study.

Better and more effective production techniques are necessary to generate more durable fibers. Pressurized gyration (PG) is a successful and innovative fiber production technique, through which rotation speed and gas pressure are used and homogenous fibers in the desired diameter and core-sheet configuration can be produced in high yield [33]. By managing several variables, including the speed of rotation of the device, applied pressure, and the polymer used, fibers with suitable properties can be obtained easily [34–36].

In this study, Cur was loaded into ZIF-8 NPs, which are considered promising carriers for enhancing bioavailability and therapeutic efficacy while reducing side effects, resulting in the formulation of Cur@ZIF-8 NPs. Subsequently, the Cur@ZIF-8 NPs were embedded into PCL fibers via the PG method. PCL fibers were selected due to their capacity to incorporate various chemotherapeutic agents and their ease of transdermal application. The physicochemical characteristics of the produced Cur@ZIF-8 NPs-embedded PCL fibers were determined using Fourier-transform infrared spectroscopy (FTIR), scanning electron microscopy (SEM), transmission electron microscopy (TEM), thermogravimetric analysis (TGA), X-ray powder diffraction (XRD), zeta potential measurement, in vitro degradation assays, differential scanning calorimetry (DSC), drug encapsulation efficiency, and in vitro drug release studies. The effects on cell viability were evaluated by the 3-(4,5-dimethylthiazol-2-yl)-2,5-diphenyltetrazolium bromide (MTT) assay, while the impact on apoptosis was assessed using the Annexin V apoptosis assay (Graphical Abstract).

2 | Results and Discussion

2.1 | Structural and Morphological Features

SEM and TEM images were used to assess the size and shape of the prepared samples; the findings are displayed in Figure 1. TEM analyses of the Cur@ZIF-8 and pure ZIF-8 NPs samples were performed to determine the size, shape, and other morphological features of the NPs. The TEM and selected area electron diffraction (SAED) pictures of ZIF-8 NPs demonstrated that the near-monodisperse, completely hexagonal crystalline diffraction pattern of the pure ZIF-8 NPs was observed (Figure 1A). The average is 25 nm when the diagonals of each particle were measured.

In SAED and TEM images of Cur@ZIF-8 NP (Figure 1B), NPs did not show a crystalline diffraction pattern but had a larger particle size than that of the pure ZIF-8 NPs. This was due to the amorphous state of Cur in ZIF-8 NPs, which disturbed and expanded the ZIF-8 crystalline structure. TEM images of pure ZIF-8 and Cur@ZIF-8 NPs at the same magnifications showed that the diagonal particle size of the Cur@ZIF-8 NPs was over 200 nm, which is almost eight times larger than the ZIF-8 NPs. This verified that ZIF-8 NPs included Cur.

In the second step of the experimental sequence, fibers were formed by PG with and without Cur@ZIF-8 NPs. The effects of PG on the fiber size and shape of pure and Cur@ZIF-8-embedded PCL fiber were investigated by SEM, and the results are presented in Figure 1.

The findings from the PG experiment showed that the incorporation of Cur@ZIF-8 NPs into a 12% PCL solution did not compromise the homogeneity of the mixture but did result in the formation of beaded fibers. When Cur@ZIF-8 NPs were added to the virgin 12% PCL fibers, the result was an increase in diameter from 5.3 ± 2 μm to 6.9 ± 2 μm (Figure 1D). The increase in fiber diameter signifies the loading of Cur@ZIF-8 NPs. The inclusion of Cur@ZIF-8 NPs in a 12% PCL solution did not affect the homogeneous distribution of the fibers. Its bigger diameter may also be due to the Cur@ZIF-8 NPs-embedded PCL fiber manufacturing solution's increased surface tension. The results of this investigation show that, in contrast to virgin PCL solution, the Cur@ZIF-8 NPs-embedded PCL solution has a higher surface tension and, hence, a larger fiber diameter (Table S1). From the morphology results for the fibers, it is clear that Cur@ZIF-8 NPs are successfully retained inside the fibers. The transformation of Cur from yellow to orange indicated its encapsulation within ZIF-8 frameworks (Figure S1).

2.2 | Fourier Transforms Infrared Spectroscopy (FTIR)

Figure 2A displays the FTIR spectra of pure PCL fiber, Cur, ZIF-8 NP, Cur@ZIF-8 NP, and embedded fiber with Cur@ZIF-8 NPs. The C—O—C stretching vibrations, aromatic C—O stretching vibrations, C═O and C═C vibrations, aromatic C═C stretching, and phenolic O—H stretching vibration were responsible for the peaks in the Cur spectrum located at 1025, 1259, 1488, 1625, and 3502 cm^{-1}, respectively [37, 38]. Zn—N symmetric stretching was identified as the band at 420 cm^{-1} in the ZIF-8 FTIR spectra. The C—H bending mode was associated with the peak at 757 cm^{-1}. The signal for ═C—H bending was detected at 1145 cm^{-1}. The full stretching of the ring was detected between 1311 and 1428 cm^{-1} [39–41]. The peaks of the Cur@ZIF-8 NPs were at 420, 1145, 1180, 1309, and 1423 cm^{-1}, which are related to the data above [42]. The C═O—C stretching vibration was identified as the source of the distinctive peak at 1162 cm^{-1} in the virgin PCL fiber spectra. The band seen at 1238 cm^{-1} was associated with an asymmetric stretching vibration of C—O—C. Stretching vibrations C—C and C—O were located at 1294 cm^{-1}. The C═O stretching vibration corresponds to the band at 1720 cm^{-1}. Asymmetric CH_2 stretching was attributed to the peak at 2942, while symmetrical CH_2 stretching was observed at 2865 cm^{-1} [43, 44]. The FTIR measurements of Cur@ZIF-8 NPs-embedded fiber were consistent with Cur, ZIF-8, and virgin PCL fiber. As a result, the outcomes demonstrate that Cur was loaded into the system effectively.

2.3 | X-Ray Powder Diffraction

The diffraction diagrams of all samples are shown in Figure 2B. The characteristic peaks of ZIF-8 NPs correspond to the values $2\theta = 7.4°$, 10.5°, 12.8°, 17.8°, and 18.1°. The characteristic peaks of Cur@ZIF-8s were measured at $2\theta = 7.4°$, 10.4°, 12.8°, and 18.1°. The similarity of the characteristic peaks of pureZIF-8 and Cur@ZIF-8 NPs was found to be consistent with the literature [45]. The fact that XRD analysis of Cur@ZIF-8 NPs showed similar results with the characteristic peaks of ZIF-8 NPs indicates that Cur does not affect the ZIF-8 crystal structure. The XRD analysis of the pure ZIF-8 and Cur@ZIF-8 NPs was also performed to evaluate if any morphological change occurred after Cur loading. When the XRD spectra of the NPs were compared (Figure 2B,iii), they have the same form and possess the same crystalline peaks. It is notable that the presence of Cur in the ZIF-8 NPs was in the amorphous state and thus did not disturb the ZIF-8 crystalline structure. XRD results are consistent with the thermal analysis results [46]. It has been observed that the characteristic peaks of PCL polymer form sharp peaks at $2\theta = 21.4°$ and 23.8°, respectively. After the Cur@ZIF-8 NPs were added to polymeric patches, the PCL crystal's crystalline peaks remained the same. This shows that the PCL crystalline structure was not changed. Also, the disappearance of all Cur and ZIF-8 NPs' crystal peaks indicates the Cur@ZIF-8 crystallinity was reduced when the drug was embedded in the polymeric vehicle. This means that the NPs were distributed out in an amorphous way [43, 47].

2.4 | Differential Scanning Calorimetry (DSC)

In the DSC thermogram (Figure S2A(a)), Cur had a melting point of 174°C. However, Cur@ZIF-8 NPs did not show any melting endotherm (Figure S2), a possible explanation that is an amorphous form of Cur in NPs. The intermolecular interaction between Cur and ZIF-8 suppressed the Cur crystallinity resulting in a homogeneous distribution in NPs. Notably, the homogeneous release of drugs in amorphous form is one of the most promising properties in drug delivery strategy. The melting temperature of both the pure and Cur@ZIF-8 NPs-embedded PCL fibers was between 65.5 and 66.33°C. There was no T_m peak of Cur in the thermogram of the Cur@ZIF-8 NPs-embedded PCL fibers, indicating that the majority of the Cur@ZIF-8 NP was dispersed amorphously in the PCL fibers and the amount of crystalline Cur was negligible [48].

2.5 | Thermal Analysis of Cur@ZIF-8 NPs

The thermal behavior and composition of materials are effectively investigated by TGA. The thermogravimetric property and thermal stability of produced ZIF-8 NPs were investigated with TGA. As pure Cur and ZIF-8 NPs have significantly different thermal behavior, the compositional analysis of Cur@ZIF-8 NPs was performed by applying the TGA technique (Figure S2B). The

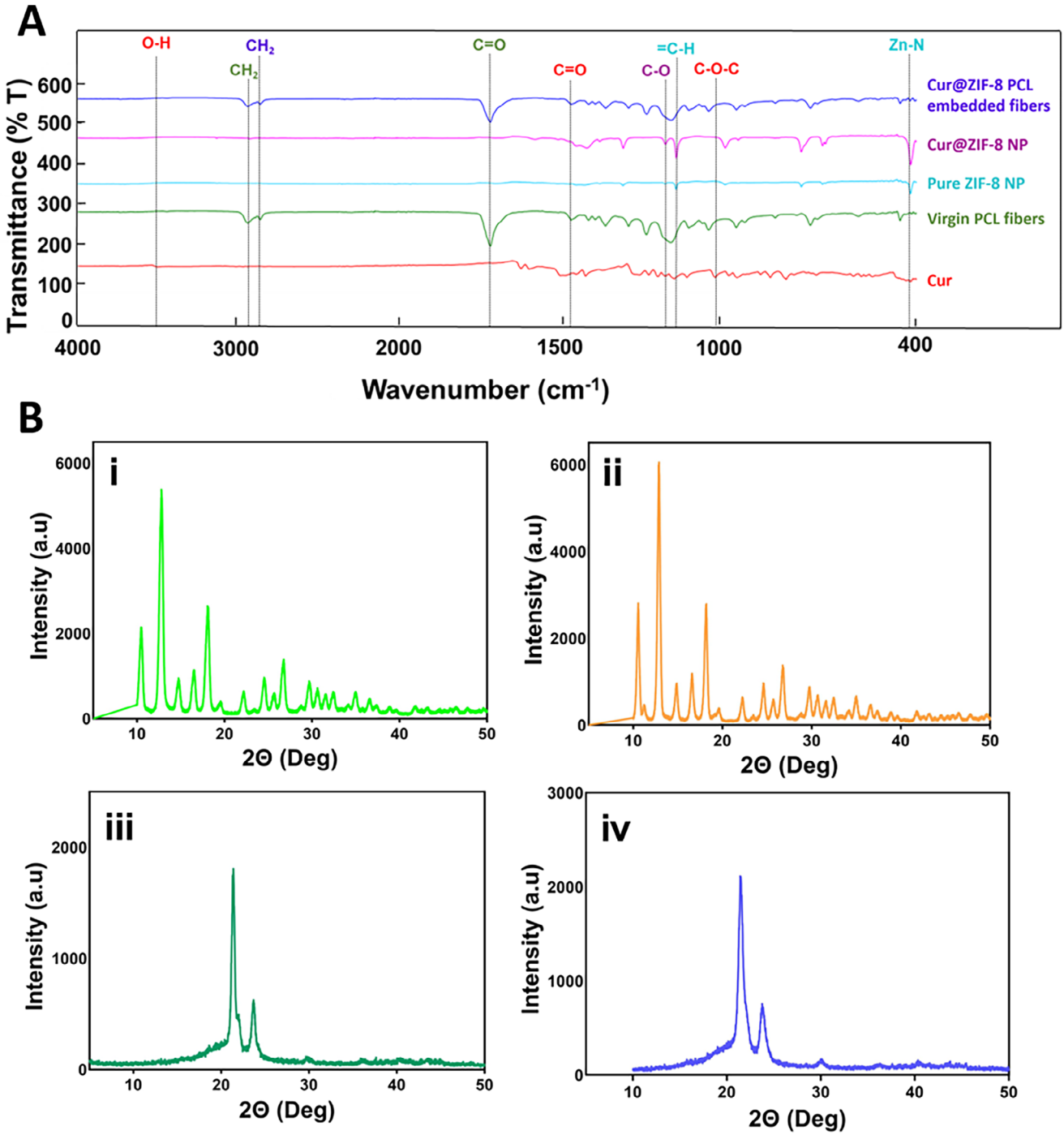

FIGURE 2 | FTIR and XRD results of samples. (A) FTIR spectra of Curcumin (Cur), pure zeolitic imidazolate framework-8 nanoparticle (Pure ZIF-8 NP), Cur-loaded zeolitic imidazolate framework-8 nanoparticle (Cur@ZIF-8 NP), virgin PCL fibers, and Cur@ZIF-8 NP-embedded PCL fibers. (B) XRD patterns of (i) pure zeolitic imidazolate framework-8 nanoparticle (Pure ZIF-8 NP), (ii) curcumin-loaded zeolitic imidazolate framework-8 nanoparticles (Cur@ZIF-8 NPs), (iii) virgin polycaprolactone (PCL) fibers, and (iv) Cur@ZIF-8 NPs-embedded PCL fibers.

main weight loss step of Cur, corresponding to a 42.5% weight loss, was observed between 200°C and 445°C (Figure S2B(A)) [38]. However, the main weight loss of ZIF-8 NPs was observed at very high decomposition temperatures of between 580°C and 620°C with 6.3% weight loss (Figure S2B(B)). In the TG curve of Cur@ZIF-8 NPs, the weight-loss temperature of Cur started at a much higher temperature compared to its pure form (331°C), corresponding to 5.2% of the sample. The percentage of Cur was calculated to be approximately 3% of Cur@ZIF-8 NPs.

The characteristic weight loss steps of the components of the material more clearly appear in their derivative TG curves (DTG) (Figure S2C). Furthermore, direct quantitative measurements of the components' thermal stability can be obtained from the region under the DTG peaks and their respective temperatures. Therefore, important data regarding the physical interaction that exists between Cur and ZIF-8 NPs was obtained by comparing the DTG peaks and temperatures. The DTG peak temperature of Cur in Cur@ZIF-8 NPs shifted to a higher temperature from

TABLE 1 | The Cur EE%, loading amount (μg/mg), the maximum release (%), and maximum release amount (μg/mg) of samples.

Sample	Encapsulation efficiency (%)	Loading amount (μg/mg)	Maximum release (%)	Maximum release amount (μg/mg)
Cur@ZIF-8 NPs	89.4	280.47	100% (ph 7.4)	280.47
			100% (ph 5.5)	280.47
Cur@ZIF-8 @PCL fibers	84.6	265.41	99.9% (ph 7.4)	262.76
			100% (ph 5.5)	265.41

386°C with a maximum weight loss rate of 5.44%/min to 404°C with a weight loss rate of 0.77%/min, while the values of ZIF-8 NPs remained unchanged. These results demonstrate that Cur exhibited enhanced thermal stability when encapsulated within the ZIF-8 structure. In this context, thermal stability refers to the resistance of Cur against thermal degradation, which was evaluated under controlled heating conditions via TGA and DTG analysis. The shift in degradation temperature and the reduced decomposition rate are attributed to intermolecular interactions and physical confinement within the porous ZIF-8 framework. This outcome agrees with Tiwary et al.'s findings [38].

2.6 | Nanoparticle Size and Zeta Potential

Both the pure ZIF-8 NPs and the Cur@ZIF-8 NPs had their zeta potential and particle sizes values evaluated. Small particle sizes have a profound impact on the diagnosis and treatment of different diseases due to their exceptional features such as controlled drug release, biocompatibility and high drug loading capacity. The Cur@ZIF-8 NPs have a size of 194.2 ± 28.5 nm (Figure 1), which enables them to circulate in the blood for extended periods, and they tend to accumulate in tumor regions because of their larger pores in the blood vessels. The measurement of zeta potential for pure ZIF-8 NPs was found to be −27.3 ± 5.2 mV, which suggests that the nanoparticles were evenly dispersed and stable before loading Cur to target breast cancer [49]. This information is critical in understanding the behavior and effectiveness of the nanoparticles in drug delivery applications. After loading with Cur, the zeta potential of the ZIF-8 NPs was increased to −18.8 ± 3.7 mV (Figure S3). The increment was associated with the hydrogen bonds amid the carbonyl, ether, and hydroxyl groups in the chemical structure of Cur [50]. The high zeta potential of the nanoparticles played a crucial role in significantly enhancing their stability in an aqueous medium by generating powerful electrostatic repulsion forces. When comparing the properties of nanoparticles, it has been observed that those with a negative charge tend to display improved stability in colloidal form [51]. Additionally, negative charge nanoparticles exhibit longer circulation time in the bloodstream and show lower toxicity towards healthy cells when compared to positively charged nanoparticles [52].

2.7 | In Vitro Drug Release

In vitro drug release tests were done for Cur@ZIF-8 NPs and Cur@ZIF-8 NPs-embedded PCL fiber samples at different pHs (5.5 and 7.4). Initially, linear standard calibration curves were established for Cur, followed by the determination of encapsulation efficiencies (EE) for the samples. The %EE of Cur in Cur@ZIF-8 NPs was 89.4% and it was slightly decreased to 84.6% after loading Cur@ZIF-8 NPs in PCL fibers. The release profiles of the samples were made by imitating physiological conditions at 37°C for 14 days. The Cur EE% and loading amount (μg mg^{-1}), as well as the maximum release (%) and maximum release amount (μg mg^{-1}), are presented in Table 1. Release results at 14 days and the first 48 h were shown in Figure 3. Cur@ZIF-8 NPs exhibited burst release, releasing 52.3% on day 1 (Figure 3B). Cur@ZIF-8 NPs-embedded PCL fiber also released the same rate as Cur@ZIF-8, but the amount of Cur released was lower. Cur@ZIF-8 NPs and Cur@ZIF-8 NPs-embedded PCL fibers showed similar release profiles at different pHs. However, the initial release rate was slightly higher under acidic conditions, consistent with the expected behavior of ZIF-8-based systems, which can undergo partial degradation in acidic environments. In the first 48 h, Cur@ZIF-8 NPs-embedded PCL fiber released 58% at pH 5.5, while it released 54% at pH 7.4. While the pH sensitivity observed in the system is relatively limited, the findings suggest that ZIF-8 remains susceptible to degradation under acidic conditions. Nevertheless, encapsulation within the PCL matrix effectively attenuates this pH-induced degradation, thereby promoting a more controlled and sustained release profile. This strategy may offer significant advantages for drug delivery applications by extending the systemic circulation time of curcumin, reducing off-target effects on healthy tissues, and enhancing its prolonged therapeutic availability. Furthermore, even a slight enhancement in release under acidic conditions could contribute to improved therapeutic efficiency in the acidic tumor microenvironment [15].

After analyzing the regression value of zero and first-order drug release, it was found that the data fits well with first-order, second-order, Higuchi, and Hixson-Crowell models for all pH values (Table 2). This indicates that the release profile of the drug from the delivery systems, which contain both hydrophobic Cur dispersed in porous matrices of Cur@ZIF-8 NPs and Cur@ZIF-8 NPs-embedded PCL fibers, is proportional to the amount of drug remaining inside the delivery system [53]. Therefore, the drug will be released at rates proportional to the remaining drug concentration. The drug release data indicated that the Higuchi model was applicable to Cur@ZIF-8 NPs and Cur@ZIF-8 NPs-embedded PCL fibers at a pH of 5.5, with a regression value greater than 0.9. This suggests that Cur release both from Cur@ZIF-8 NPs and Cur@ZIF-8 NPs-embedded PCL fibers is largely controlled by diffusion [54].

However, at pH 7.4, the Higuchi model provides a higher R^2 than Korsmeyer-Peppas, indicating that the release is diffusion con-

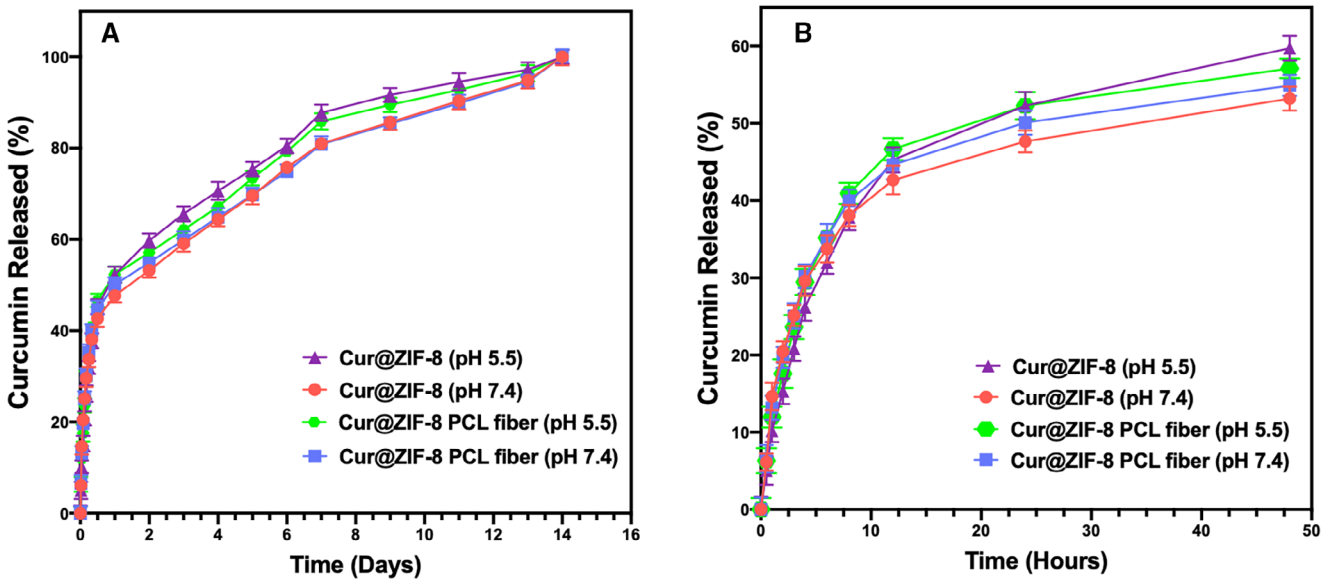

FIGURE 3 | (A) Percentage cumulative Curcumin (Cur) release from the samples in PBS solutions at selected time intervals and (B) percentage cumulative Cur burst release from the samples in PBS solutions at selected time intervals. Data represent the mean ± standard error of the mean ($n = 3$).

TABLE 2 | Drug release kinetics of each formulation.

	R^2						
Formulations	**Zero-order**	**First-order**	**Second-order**	**Weibull**	**Higuchi**	**Korsmeyer–Peppas**	**Hixson–Crowell**
Cur@ZIF-8 (pH 5.5)	0.780	0.973	0.988	0.776	0.936	0.767	0.944
Cur@ZIF-8 (pH 7.4)	0.824	0.919	0.977	0.755	0.951	0.706	0.917
Cur@ZIF-8 PCL (pH 5.5)	0.789	0.952	0.983	0.767	0.934	0.725	0.932
Cur@ZIF-8 PCL (pH 7.4)	0.808	0.909	0.978	0.757	0.940	0.704	0.912

trolled for both Cur@ZIF-8 NPs and Cur@ZIF-8 NPs-embedded PCL [55]. Subsequently, it has been observed that the decrease in pH from 7.4 to 5.5 leads to an increase in the amount of Cur release due to the dissolution of ZIF-8 NPs. The first-order, second-order, and Hixson-Crowell model is best suited for the pH 5.5 data and supports the notion that the increase in Cur release is due to the dissolution of ZIF-8 embedded in PCL, as it suggests an erosion-dependent release mechanism. The proposed kinetic models clearly indicate a direct correlation between decreasing pH levels and an increase in drug release constants.

2.8 | In Vitro Degradation Test

The degradation behavior of NPs and PCL fibers was evaluated at the determined time intervals (on hours 1, 4, 8, and 12, and on days 5, 9, 13, 17, 21, 24, 29, 33, 37, and 41) for 41 days, and the results are given in Figure 4. All samples except Cur@ZIF-8 NPs-embedded PCL fiber lost significant weight on the first day. While Pure ZIF-8 NPs completed their degradation on day 24, Cur@ZIF-8 NPs continued to degrade until day 41 (~97%). Cur@ZIF-8 NPs-embedded PCL fiber showed lower and slower degradation behavior in comparison to all other samples (~76%). It was

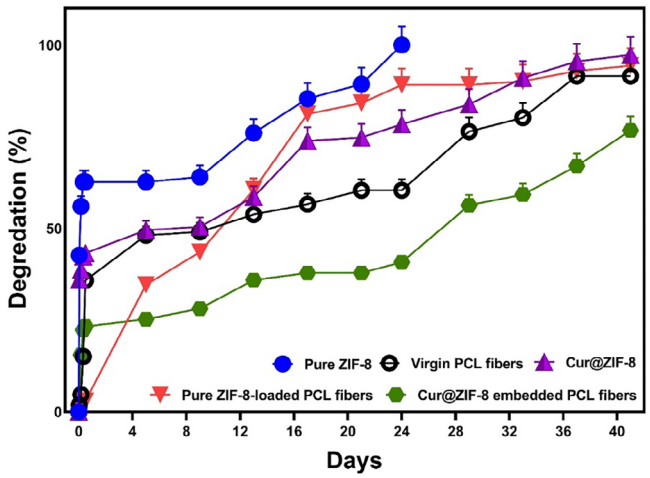

FIGURE 4 | Degradation behaviors of all samples in PBS at 37°C (pH = 7.4). Data represent the mean ± standard error of the mean ($n = 3$).

determined that this situation is related to the strong hydrogen bond and hydrophobic interaction between ZIF-8 crystals and PCL fibers [56]. Since the study aims to achieve controlled release

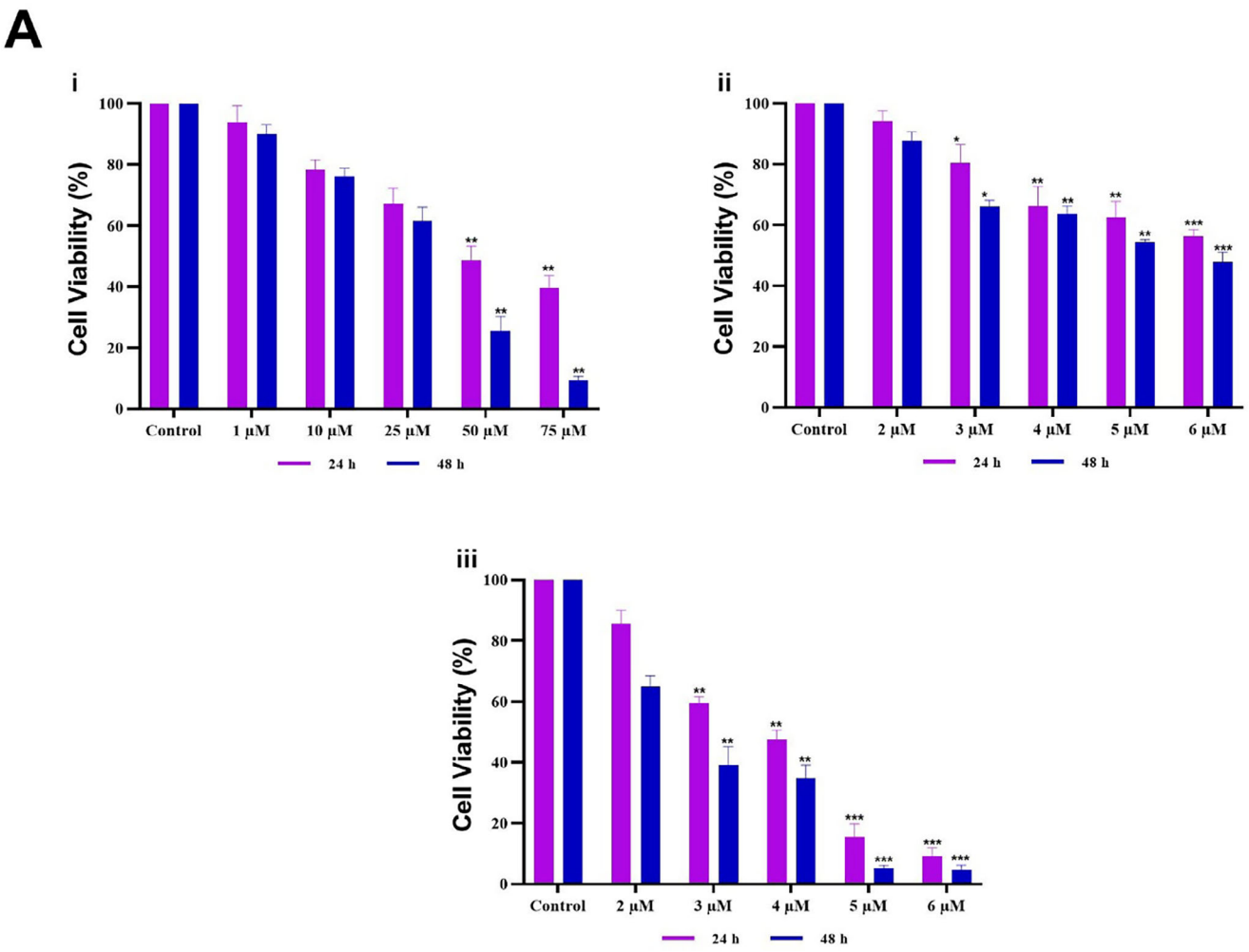

FIGURE 5 | In vitro cell culture studies. (A) The viability levels of (i) powdered Curcumin (Cur), (ii) pure zeolitic imidazolate framework-8 nanoparticle (Pure ZIF-8 NP), and (iii) Cur-loaded zeolitic imidazolate framework-8 nanoparticle (Cur@ZIF-8 NP) on MCF-7 cell lines for 24 and 48 h. $^{*}p < 0.05$, $^{**}p < 0.01$, and $^{***}p < 0.001$ compared to the control group. (B) Flow cytometric analysis of the Annexin-V positive cell (i), apoptosis (ii), and necrosis (iii) percentages following Annexin V-FITC/PI staining on the MCF-7 cell line. $^{**}p < 0.01$ and $^{****}p < 0.001$ compared to the control group. Data represent the mean ± standard error of the mean ($n = 3$).

in the blood and rapid release in the cancer microenvironment, this shows that the expected result was achieved.

2.9 | In Vitro Cell Culture Studies

2.9.1 | Cell Viability

In this study, IC_{50} values were used as the treatment dose and MTT analysis was performed to determine these doses. The effects of powdered Cur (Figures 5Ai), pure ZIF-8 NPs (Figures 5Aii), and Cur@ZIF-8 NPs (Figures 5Aiii) groups on cell viability were examined in a dose-dependent manner. MCF-7 cells were exposed to varying dosages of powdered Cur (1–75 µM) and Cur@ZIF-8 NPs (2–6 µM). IC_{50} values were determined as 51.05 µM (24 h) and 31.45 µM (48 h) for powdered Cur; 3.36 µM (24 h) and 2.59 µM (48 h) for Cur@ZIF-8 NPs, which indicate the IC_{50} of Cur@ZIF-8 NPs was lower than powdered Cur on MCF-7 cells (Figure S4). The same weight percentage of Cur@ZIF-8 NPs was utilized in order to investigate the impact of pure ZIF-8 on cell survival. Cell viability was lowered by pure ZIF-8 NPs in a dose-dependent way. This is consistent with the literature [57]. The study reveals that increasing the drug dose is associated with decreased viability in MCF-7 cells and reveals that the effectiveness of the drug is dose-dependent. It has also been observed that longer exposure reduces cell viability. Compared to the control group, viability at 48 h was notably lower in all samples compared to 24 h ($^{*}p < 0.05$). Cur@ZIF-8 NPs have more bioavailability than powdered Cur and can penetrate the cells to deliver its effect [58]. Therefore, the nanotechnology-based approach can be a promising solution to the pharmacokinetic challenges associated with Cur.

2.9.2 | Annexin V Apoptosis

Following treatment of MCF 7-cells with powdered Cur, pure ZIF-8 NPs, and Cur@ZIF-8 NPs for 48 h, the apoptotic cell ratios were 64.16%, 4.32%, and 34.25%, respectively. The Cur and Cur@ZIF-8 groups had a statistically significant increase

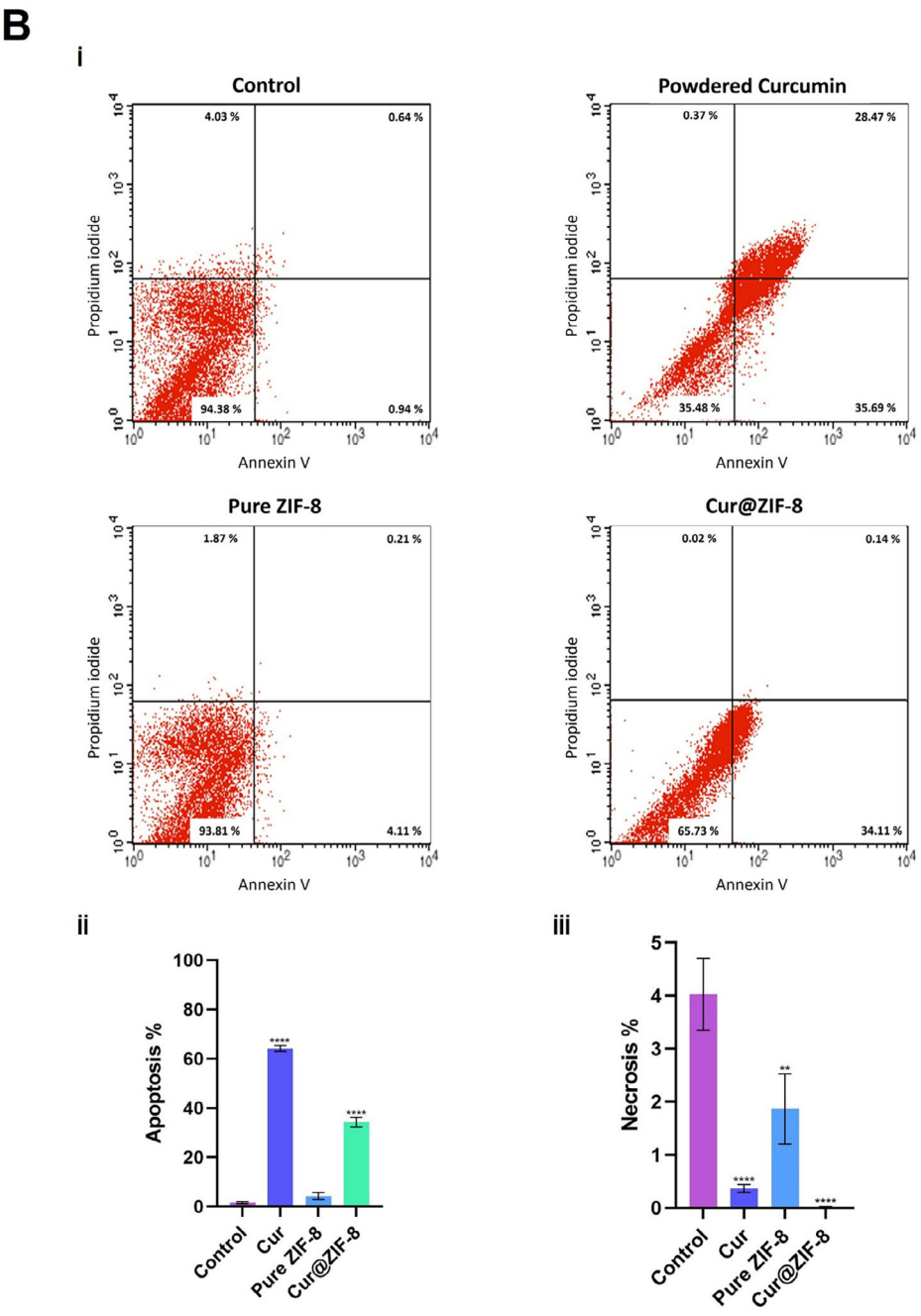

FIGURE 5 | (Continued)

in comparison to the control group (****$p < 0.0001$). Reactive oxygen species generation is directly correlated with apoptosis. This causes MCF-7 cells to undergo apoptosis and experience mitochondrial malfunction [59]. On the other hand, the necrotic cell ratios were 0.37%, 1.87%, and 0.02%, respectively. All three treatment groups showed a substantial decrease (**$p < 0.01$ and ****$p < 0.001$) when compared to the control group. Necrosis and apoptosis are two distinct processes that lead to cell death. In apoptosis, surrounding cells are not affected and apoptotic cells can be digested by macrophages. On the other hand, necrosis causes the cell to release many molecules that trigger the inflammatory response, thereby damaging healthy cells. According to the result of this research, Cur@ZIF-8 NPs decrease necrosis, which increases apoptosis—the regulated, planned death of cells (Figure 5B). This effect proves that it has a pH-sensitive effect on the acidic microenvironment of the MCF-7 cancer cell resulting in a higher rate of apoptosis [60].

3 | Experimental Section/Methods

3.1 | Materials

Zinc (II) nitrate hexahydrate ($Zn(NO_3)_2$-$6H_2O$, Mw: 297.5 g mol^{-1}), 2-methylimidazole (Mw: 82.10 g mol^{-1}), polycaprolactone (PCL, Mw: ~80 000), methanol (Mw: 32.042 g mol^{-1}), and Cur (Mw: 368.4 g mol^{-1}) were supplied by Sigma-Aldrich (UK).

TABLE 3 | Main parameters of fiber production using pressurized gyration. Fibers were produced at 33 ± 2°C and 33 ± 2% temperature and humidity, respectively.

Samples	Rotation speed (rpm)	Gas pressure (MPa)
PCL fibers (8%, w/v)	12 000	0.3
PCL fibers (12%, w/v)	12 000	0.3
PCL fibers (16%, w/v)	12 000	0.3
Cur@ZIF-8 NPs-embedded 12% PCL fibers (12%, w/v)	12 000	0.3

3.2 | ZIF-8 Nanoparticle Synthesis

A total of 50 mL of methanol was used to dissolve 1.05 g (3.53 mmol) of $Zn(NO_3)_2.6H_2O$ in order to create the first solution. The second one was obtained with the dissolution of 2.34 g (28.3 mmol) 2-methylimidazole in 50 mL of methanol, to which the first solution was added. The last obtained solution was mixed continuously for 1 h at room temperature (25°C). Centrifugation and washing with methanol were applied three times to the synthesized ZIF-8 NPs, and the drying process at 80°C for 24 h was carried out [61].

3.3 | Cur@ZIF-8 Nanoparticle Synthesis

Cur@ZIF-8 NPs were prepared by dissolving 80 mg of Cur and 2.34 g (28.3 mmol) of 2-methylimidazole with 50 mL of methanol. Subsequently, 1.05 g of (3.53 mmol) $Zn(NO_3)_2.6H_2O$ solution was dissolved in the same amount of methanol. Cur@ZIF-8 NPs were formed after centrifugation and three times washing with methanol [62].

3.4 | Preparation of Solutions

Three different concentrations of PCL solutions (8%, 12%, 16%, w/v) were made by stirring PCL in chloroform/methanol (3:1, v/v) solution for almost 1 h at room temperature. The viscosity, surface tension, and density of each solution were measured using a viscometer (DV-E, Brookfield AMETEK, USA), a force tensiometer (Sigma 703D, Attension, Germany), and a standard density flask (10 mL, Boru Cam Inc., Turkey). Before the measurements, all the equipment was calibrated. At ambient temperature (25°C), each measurement was performed three times (Table S1) [43, 63].

3.5 | Preparation of Fibers

Different PCL ratios were used to obtain the best results. Fiber production was performed at PCL ratios of 8%, 12%, and 16% (w/v), respectively, and 12% was determined as the optimized ratio. Parameters in the production of pure and Cur@ZIF-8 NPs-embedded PCL fibers by PG are shown in Table 3. Cur@ZIF-8 NPs were added to the 12% (w/v) PCL solution and mixed for 60 s to prevent Cur release from Cur@ZIF-8 NPs, and then, Cur@ZIF-8 NPs-embedded transdermal polymeric patches were produced. The PG device, which enables fiber production within seconds, is a superior method in terms of preventing ZIF-8 NPs from releasing the drug inside. The PG process was performed at a gas pressure of 0.3 MPa and a rotational speed of 12 000 rpm [64].

3.6 | Scanning Electron Microscopy (SEM)

The diameter and morphology were determined using SEM (EVO LS 10, ZEISS). For 60 s, gold was applied to the samples' surface. The applied accelerating voltage was 20 kV, and the working distance was 25 mm. Using Image software (Brocken Symmetry Software), the average diameter and diameter distribution of the fibers were determined.

3.7 | Transmission Electron Microscopy (TEM)

Transmission electron microscopy (TEM) was used to investigate the form and size distribution of pure ZIF-8 and Cur@ZIF-8 NPs. On the JEOL JEM 2100 HRTEM, TEM images were captured at an acceleration voltage of 200 kV. Using the Gatan Model 833 Orius SC200D CCD Camera, pictures were captured. The carbon support film-covered copper TEM grids (Electron Microscopy Sciences, CF200-Cu, 200 mesh) were used.

3.8 | Fourier Transforms Infrared Spectroscopy (FTIR)

FTIR measurements were utilized to analyze the confirmation of the loaded drug presence. Jasco, FT/IR 4700 spectrometer was performed for the measurement at room temperature using OPUS Viewer version 6.5 software. The transmission mode had a resolution of 4 cm^{-1} and covered the 500–4000 cm^{-1} range.

3.9 | X-Ray Powder Diffraction (XRD)

Using a D/Max-BR diffractometer (RigaKu, Tokyo, Japan), the materials' structure and crystal shape were evaluated. At a pace of 2° min^{-1}, analyses were displayed at 40 mV and 30 mA across a range of $2\theta = 5°–90°$. The software OriginPro 7.0 (OriginLab Corporation, MA, USA) was utilized to create diffractograms from the acquired data.

3.10 | Differential Scanning Calorimetry (DSC)

The morphological features of Cur@ZIF-8 NPs was investigated using differential scanning calorimetry (DSC). Measurements were performed using a Perkin Elmer Jade DSC instrument under an argon atmosphere (200 mL min^{-1}) with a 5–7 mg sample at a heating range of 10°C min^{-1}. Data were evaluated using Pyris software.

3.11 | Thermogravimetric Analysis (TGA)

Compositional analysis of NPs was performed using thermo gravimetric analysis (TGA). Additionally, derivative thermogravimetry was employed since it provides an enhanced under-

standing of the samples' weight loss patterns. On a Seiko-EXSTARTG/DTA7300 type thermal analysis equipment, TGA and DTG curves were recorded. A total of 5–7 mg of samples were measured at a heating rate of 10°C min^{-1} in a dynamic N_2 environment (200 mL min^{-1}). Muse software was applied to examine the thermal analysis results.

3.12 | Zeta Potential

Using a Malvern Zetasizer Nano ZS, dynamic light scattering (DLS) was utilized to assess zeta potential and particle size (Malvern Instruments Ltd., Worcestershire, UK). A suspension of nanoparticles was appropriately diluted in two different pH solutions (5.5 and 7.4) (1 mL each), thoroughly mixed, and then gently transfer the mixture into a 1 mL transparent zeta potential cuvette or a 4 mL polystyrene cuvette. To guarantee the repeatability of the results, measurements were made three times for each samples at the temperature of 25°C [65, 66].

3.13 | Drug Encapsulation Efficiency

Drug encapsulation efficiency was calculated to ascertain the drug content. The dry sample of Cur@ZIF-8 NPs was dissolved thoroughly by 50 µL of 2 M HCl. After that, the Cur solution was diluted with ethanol. A UV-visible spectrophotometer (Shimadzu UV-3600, Japan) was used to conduct a standard curve analysis on the resulting clear yellow Cur solution at 425 nm. Drug encapsulation efficiency was calculated based on the equation below [62]. The measurements were made three times for the fibers, and 5 mg of each was weighed, then dissolved in 10 mL of solvent mixes in separate vials. To ensure the complete release of the drug from the fibers into the solvent mixtures, the vials were lightly stirred for 1.5 h. A UV-visible spectrophotometer was used to measure the outcomes using 1 mL of each solution (Shimadzu UV-3600, Japan).

$$\text{Drug encapsulation efficiency (\%)} = (\text{amount of loaded drug})/(\text{total amount of feeding drug}) \times 100\%$$

3.14 | In Vitro Drug Release

To investigate the drug release properties, in vitro drug release kinetics were applied. Cur solutions were prepared independently at five different concentrations (0.2, 0.4, 0.6, 0.8, and 1 µg mL^{-1}) using phosphate-buffered saline (PBS) in order to create a linear calibration curve for each one. The samples prepared to weigh approximately 5 mg were immersed in 1 mL of PBS (pH 7.4 and 5.5 at 37°C). It was studied at pH 7.4 and 5.5 to obtain a pH-sensitive drug release. Following that, samples were kept on a rotary shaker at 250 rpm, 37°C throughout the testing process. At the determined times (0, 0.25, 0.5, 1, 2, 3, 4, 6, 8, 12, 24, 48, 72, 96, 120, 144 h and 7, 9, 11, 13, 14 days), 1 mL of sample was removed and 1 mL of fresh PBS was added. The Eppendorf vials were filled with PBS in order to continue the drug release test. A Shimadzu UV-3600 UV spectrophotometer (Japan) was used to examine the drug's release profile. Because Cur gives its characteristic peak at 425 nm, this wavelength was taken into account during the release analysis [45]. The Kinet DS Software (v.3.0, Santa Cruz, California, USA) was used to calculate with respect to seven kinetic models (Zero-order, First-order, Second-order, Weibull, Higuchi, Korsmeyer-Peppas, and Hixson-Crowell) based on release patterns.

3.15 | In Vitro Degradation

Each sample, which was dried, had an initial weight of approximately 5 mg. The samples that were prepared were stored in a shaking incubator with PBS (pH 7.4) at 37°C [67]. The samples were measured at 1, 4, 8, and 12 h and on days 5, 9, 13, 17, 21, 24, 29, 33, 37, and 41. After each measurement, the same amount of fresh PBS solution was added as before. When the samples were removed, the water on the samples' surface was carefully taken up with filter paper. Following this step, using a vacuum dryer, the samples for each time point were dried and afterward weighed until a fixed weight was obtained. The measurements were repeated three times.

The degradation of mass loss (%) was calculated as follows:

$$\text{Degradation test } (\%) = [(W_0 - W_t) / W_0] \times 100$$

where W_t is the weight of the deteriorated sample at the incubation period, and W_0 is the initial weight (t).

3.16 | In Vitro Cell Culture

In a humidified 5% CO_2 atmosphere at 37°C, human breast cancer MCF-7 cells were cultured in DMEM supplemented with L-glutamine (Capricorn Scientific, Germany) media containing 10% fetal bovine serum (FBS) and 1% penicillin-streptomycin (P/S) (Thermo, Gibco). Our study groups in these cells were determined as Cur@ZIF-8, pure ZIF-8, and powdered Cur groups.

3.16.1 | Cell Viability Assay

The viability of the powdered Cur, pure ZIF-8 NP, and Cur@ZIF-8, groups were assessed by MTT assay at 24 and 48 h [68]. 96-well plates were seeded with MCF-7 cells at a density of 1×10^4 cells per well ($n = 4$), and the plates were incubated for a full day. After the whole 24 h, the medium on the cells was taken off, and new medium was added to the control group and treatment groups. In the next stage, to determine the viability of the samples, 10 µL of MTT agent was added to the wells at 24 and 48 h. After incubating for 3 h, the medium was taken out of the plate and 100 µL of DMSO was added. Following a 5 min incubation period in the shaker, the plate's absorbance at 570 nm was determined. The inhibitory concentration 50 (IC_{50}) values of the Cur@ZIF-8 and powdered Cur were calculated with CompuSyn (Paramus, USA). Experiments were repeated three times.

3.16.2 | Annexin V Apoptosis Assay

Observing the guidelines provided by the manufacturer, propidium iodide (PI) detection kit (SONY Biotechnology, USA) and

annexin V-fluorescein isothiocyanate (Annexin V-FITC) were used to assess necrosis and apoptosis using flow cytometry [68]. Briefly, approximately 5×10^5 cells treated with IC_{50} doses of powdered Cur (31.45 μM for 48 h) and Cur@ZIF-8 (2.59 μM for 48 h) were used to investigate the impact of pure ZIF-8 on apoptosis and necrosis, an equal weight of pure ZIF-8 was used as the Cur@ZIF-8. After 48 h, the cells were collected. A volume of 500 μL of 1 × Annexin binding buffer was added to all groups. Next, 5 μL of Annexin V-FITC and 3 μL of the PI viability staining dye were added and mixed. All tubes underwent incubation in the dark at room temperature for 30 min. The FACS Calibur flow cytometer was used to process the cells, and Cell Search software (BD Biosciences, USA) was used to calculate the data. Applying unstained, Annexin V, and PI controls, an adjustment was first made. At last, analysis was carried out on the fluorescence that represented the extracted cells' apoptosis, necrosis, and vitality. Experiments were repeated three times.

3.17 | Statistical Analysis

The data obtained from the measures were statistically analyzed using Graphpad Prism 8 software (Graphpad, San Diego, CA, USA). With the exception of SEM data, which are shown as mean ± standard deviation, each outcome was shown as the average ± standard error of the average. An analysis of variance (ANOVA) with a 95% confidence interval and Tukey's post hoc test were utilized to examine the relationships between different groups in cell culture. Whereas substantial differences were allowed for $p < 0.05$ values, significant differences were not accepted for $p > 0.05$ values.

4 | Conclusions

The new strategies for cancer treatment may be a good alternative to cancer drugs with high cytotoxic side effects for the microenvironment. Here, a new pH-responsive method has been shown for BC. The SEM and TEM images showed that pure ZIF-8 NPs have a crystal diffraction pattern and perfect hexagonal form with almost one-dimensional distribution. Cur@ZIF-8 NPs were homogenously produced in the size of ~200 nm and Cur had better stability inside Cur@ZIF-8 NPs than that of the powder form. Cur@ZIF-8 NPs-embedded PCL fibers were homogenously produced in the size of ~7 μm by PG and usable treatment patches were generated. Cur was released in a controlled manner for 14 days fitting the first-order, second-order, Higuchi, and Hixson-Crowell models and its efficiency was increased in the acidic microenvironment that is characteristic of cancer. Cur@ZIF-8 NPs have more bioavailability than powdered Cur and can penetrate the cells to deliver their anticancer effects on MCF-7 human breast cancer cells. Cur@ZIF-8 NPs-embedded transdermal polymeric patches have a pH-sensitive effect and lead MCF-7 cells to apoptosis by reducing necrosis. Based on the ZIF-8 nano-carrier system, this work presents a release mechanism that is mildly responsive to acidic conditions and offers synergistic anticancer functionality, thereby paving the way for the potential clinical application of curcumin in breast cancer therapy. However, certain limitations must be acknowledged. The biocompatibility and cytotoxicity of Cur@ZIF-8 NPs were assessed only in cancer cells; further investigations are needed to evaluate their effects on healthy cell lines and normal tissues. Additionally, in vivo experiments and long-term toxicity studies will be critical for determining the clinical translation potential of the developed formulation. Hence, this potential and exciting application will be a pioneer for the research of new approaches.

Acknowledgments

This project was supported by a TUBITAK 2209-A Research Projects Program Grant (2209-A, 2022/-1, No:1919B012208840, Scientific and Technological Research Council of Turkey-TUBITAK). H.B.Y. acknowledges TUBITAK 2211-A and 2250 for her scholarships. The authors dedicate this article to the memory of Turkish citizens, who lost their lives in the earthquakes of Pazarcık and Elbistan-Kahramanmaras, and Hatay, Türkiye on February 06, 2023.

Conflicts of Interest

The authors declare no conflicts of interest.

Data Availability Statement

The data that support the findings of this study are available from the corresponding author upon reasonable request.

References

1. F. Bray, J. Ferlay, I. Soerjomataram, R. L. Siegel, L. A. Torre, and A. Jemal, "Global Cancer Statistics 2018: GLOBOCAN Estimates of Incidence and Mortality Worldwide for 36 Cancers in 185 Countries," *CA: A Cancer Journal for Clinicians* 68, no. 6 (2018): 394–424, https://doi.org/10.3322/caac.21492.

2. Y. Park, J. Jeong, S. Seong, and W. Kim, "In Silico Evaluation of Natural Compounds for an Acidic Extracellular Environment in Human Breast Cancer," *Cells* 10, no. 10 (2021): 2673, https://doi.org/10.3390/cells10102673.

3. J. Ferlay, M. Colombet, I. Soerjomataram, et al., "Cancer Statistics for the Year 2020: An Overview," *International Journal of Cancer* 149, no. 4 (2021): 778–789, https://doi.org/10.1002/ijc.33975.

4. X. Mi, M. Hu, M. Dong, et al., "Folic Acid Decorated Zeolitic Imidazolate Framework (ZIF-8) Loaded With Baicalin as a Nano-Drug Delivery System for Breast Cancer Therapy," *International Journal of Nanomedicine* 16 (2021): 8337–8352, https://doi.org/10.2147/IJN.S340764.

5. F. Topal, B. Ertas, E. Guler, et al., "A Novel Multi-Target Strategy for Alzheimer's Disease Treatment via Sublingual Route: Donepezil/Memantine/Curcumin-Loaded Nanofibers," *Biomaterials Advances* 138 (2022): 212870, https://doi.org/10.1016/j.bioadv.2022.212870.

6. T. Feng, Y. Wei, R. J. Lee, and L. Zhao, "Liposomal Curcumin and Its Application in Cancer," *International Journal of Nanomedicine* 12 (2017): 6027–6044, https://doi.org/10.2147/IJN.S132434.

7. P. Sivasami and T. Hemalatha, "Augmentation of Therapeutic Potential of Curcumin Using Nanotechnology: Current Perspectives," *Artificial Cells, Nanomedicine, and Biotechnology* 46, no. S1 (2018): 1004–1015, https://doi.org/10.1080/21691401.2018.1442345.

8. A. Giordano and G. Tommonaro, "Curcumin and Cancer," *Nutrients* 11, no. 10 (2019): 2376, https://doi.org/10.3390/nu11102376.

9. L. Farhoudi, P. Kesharwani, M. Majeed, T. P. Johnston, and A. Sahebkar, "Polymeric Nanomicelles of Curcumin: Potential Applications in Cancer," *International Journal of Pharmaceutics* 617 (2022): 121622, https://doi.org/10.1016/j.ijpharm.2022.121622.

10. E. Guler, A. Nur Hazar-Yavuz, E. Tatar, et al., "Oral Empagliflozin-Loaded Tri-Layer Core-Sheath Fibers Fabricated Using Tri-Axial Electrospinning: Enhanced In Vitro and In Vivo Antidiabetic Performance," *International Journal of Pharmaceutics* 635 (2023): 122716, https://doi.org/10.1016/j.ijpharm.2023.122716.

11. S. M. S. Shahriar, J. Mondal, M. N. Hasan, V. Revuri, D. Y. Lee, and Y.-K. Lee, "Electrospinning Nanofibers for Therapeutics Delivery," *Nanomaterials* 9, no. 4 (2019): 532, https://doi.org/10.3390/nano9040532.

12. A. Luraghi, F. Peri, and L. Moroni, "Electrospinning for Drug Delivery Applications: A Review," *Journal of Controlled Release* 334 (2021): 463–484, https://doi.org/10.1016/j.jconrel.2021.04.019.

13. E. B. Polat, A. N. Hazar-Yavuz, E. Guler, et al., "Sublingual Administration of Teucrium Polium-Loaded Nanofibers With Ultra-Fast Release in the Treatment of Diabetes Mellitus: In Vitro and In Vivo Evaluation," *Journal of Pharmaceutical Sciences* 113, no. 4 (2024): 1068–1087, https://doi.org/10.1016/j.xphs.2023.10.028.

14. D. W. Chen and S. J. Liu, "Nanofibers Used for Delivery of Antimicrobial Agents," *Nanomedicine (Lond)* 10, no. 12 (2015): 1959–1971, https://doi.org/10.2217/nnm.15.46.

15. S. Abd Al-jabbar, V. Atiroğlu, R. M. Hameed, et al., "Fabrication of Dopamine Conjugated With Protein @Metal Organic Framework for Targeted Drug Delivery: A Biocompatible pH-Responsive Nanocarrier for Gemcitabine Release on MCF-7 Human Breast Cancer Cells," *Bioorganic Chemistry* 118 (2022): 105467, https://doi.org/10.1016/j.bioorg.2021.105467.

16. M. Coluccia, V. Parisse, P. Guglielmi, G. Giannini, and D. Secci, "Metal-Organic Frameworks (MOFs) as Biomolecules Drug Delivery Systems for Anticancer Purposes," *European Journal of Medicinal Chemistry* 244 (2022): 114801, https://doi.org/10.1016/j.ejmech.2022.114801.

17. Y. Li, Y. Song, W. Zhang, et al., "MOF Nanoparticles With Encapsulated Dihydroartemisinin as a Controlled Drug Delivery System for Enhanced Cancer Therapy and Mechanism Analysis," *Journal of Materials Chemistry B* 8, no. 33 (2020): 7382–7389, https://doi.org/10.1039/D0TB01330G.

18. L. R. de Moura Ferraz, A. É. G. A. Tabosa, D. D. S. da Silva Nascimento, et al., "ZIF-8 as a Promising Drug Delivery System for Benznidazole: Development, Characterization, In Vitro Dialysis Release and Cytotoxicity," *Scientific Reports* 10, no. 1 (2020): 16815, https://doi.org/10.1038/s41598-020-73848-w.

19. Y. Li, Z. Lin, X. Wang, et al., "High-Hydrophobic ZIF-8@PLA Composite Aerogel and Application for Oil-Water Separation," *Separation and Purification Technology* 270 (2021): 118794, https://doi.org/10.1016/j.seppur.2021.118794.

20. C. Zheng, Y. Wang, S. Z. F. Phua, W. Q. Lim, and Y. Zhao, "ZnO–DOX@ZIF-8 Core–Shell Nanoparticles for pH-Responsive Drug Delivery," *ACS Biomaterials Science & Engineering* 3, no. 10 (2017): 2223–2229, https://doi.org/10.1021/acsbiomaterials.7b00435.

21. L. Feng, Z. Dong, D. Tao, Y. Zhang, and Z. Liu, "The Acidic Tumor Microenvironment: A Target for Smart Cancer Nano-Theranostics," *National Science Review* 5, no. 2 (2017): 269–286, https://doi.org/10.1093/nsr/nwx102.

22. J. Zhuang, C.-H. Kuo, L.-Y. Chou, D.-Y. Liu, E. Weerapana, and C.-K. Tsung, "Optimized Metal–Organic-Framework Nanospheres for Drug Delivery: Evaluation of Small-Molecule Encapsulation," *ACS Nano* 8, no. 3 (2014): 2812–2819, https://doi.org/10.1021/nn406590q.

23. E. Guler, H. B. Yekeler, G. Parviz, et al., "Vitamin B12-Loaded Chitosan-Based Nanoparticle-Embedded Polymeric Nanofibers for Sublingual and Transdermal Applications: Two Alternative Application Routes for Vitamin B12," *International Journal of Biological Macromolecules* 258 (2024): 128635, https://doi.org/10.1016/j.ijbiomac.2023.128635.

24. L. Li, R. Hao, J. Qin, et al., "Electrospun Fibers Control Drug Delivery for Tissue Regeneration and Cancer Therapy," *Advanced Fiber Materials* 4, no. 6 (2022): 1375–1413, https://doi.org/10.1007/s42765-022-00198-9.

25. B. Pant, M. Park, and S.-J. Park, "Drug Delivery Applications of Core-Sheath Nanofibers Prepared by Coaxial Electrospinning: A Review," *Pharmaceutics* 11, no. 7 (2019): 305, https://doi.org/10.3390/pharmaceutics11070305.

26. J. Ahmed, E. Guler, G. Sinemcan Ozcan, M. .E. Cam, S. Homer-Vanniasinkam, and M. Edirisinghe, "Casein Fibres for Wound Healing," *Journal of The Royal Society Interface* 20, no. 204 (2023): 20230166, https://doi.org/10.1098/rsif.2023.0166.

27. B. Ertas, I. N. Onay, A. M. Yilmaz-Goler, B. Karademir-Yilmaz, I. Aslan, and M. E. Cam, "A Novel High-Efficiency Transdermal Patches for Combinational Therapy of Alzheimer's Disease: Donepezil/Vitamin B12-Loaded Nanofibers," *Journal of Drug Delivery Science and Technology* 89 (2023): 104963, https://doi.org/10.1016/j.jddst.2023.104963.

28. P. Grossen, D. Witzigmann, S. Sieber, and J. Huwyler, "PEG-PCL-Based Nanomedicines: A Biodegradable Drug Delivery System and Its Application," *Journal of Controlled Release* 260 (2017): 46–60, https://doi.org/10.1016/j.jconrel.2017.05.018.

29. J. Peng, J. Chen, F. Xie, et al., "Herceptin-Conjugated Paclitaxel Loaded PCL-PEG Worm-Like Nanocrystal Micelles for the Combinatorial Treatment of HER2-Positive Breast Cancer," *Biomaterials* 222 (2019): 119420, https://doi.org/10.1016/j.biomaterials.2019.119420.

30. M. Q. Khan, M. A. Alvi, H. H. Nawaz, and M. Umar, "Cancer Treatment Using Nanofibers: A Review," *Nanomaterials (Basel)* 14, no. 15 (2024): 1305, https://doi.org/10.3390/nano14151305.

31. L. Chen, A. Nabil, N. Fujisawa, E. Oe, K. Li, and M. Ebara, "A Facile, Flexible, and Multifunctional Thermo-Chemotherapy System for Customized Treatment of Drug-Resistant Breast Cancer," *Journal of Controlled Release* 363 (2023): 550–561, https://doi.org/10.1016/j.jconrel.2023.10.010.

32. R. Sridhar, S. Ravanan, J. R. Venugopal, et al., "Curcumin- and Natural Extract-Loaded Nanofibres for Potential Treatment of Lung and Breast Cancer: In Vitro Efficacy Evaluation," *Journal of Biomaterials Science* 25, no. 10 (2014): 985–998, https://doi.org/10.1080/09205063.2014.917039.

33. P. L. Heseltine, J. Ahmed, and M. Edirisinghe, "Developments in Pressurized Gyration for the Mass Production of Polymeric Fibers," *Macromolecular Materials and Engineering* 303, no. 9 (2018): 1800218, https://doi.org/10.1002/mame.201800218.

34. J. Ahmed, M. Gultekinoglu, and M. Edirisinghe, "Bacterial Cellulose Micro-Nano Fibres for Wound Healing Applications," *Biotechnology Advances* 41 (2020): 107549, https://doi.org/10.1016/j.biotechadv.2020.107549.

35. X. Hong, M. Edirisinghe, and S. Mahalingam, "Beads, Beaded-Fibres and Fibres: Tailoring the Morphology of Poly(caprolactone) Using Pressurised Gyration," *Materials Science and Engineering: C* 69 (2016): 1373–1382, https://doi.org/10.1016/j.msec.2016.05.020.

36. Y. Dai, J. Ahmed, and M. Edirisinghe, "Pressurized Gyration: Fundamentals, Advancements, and Future," *Macromolecular Materials and Engineering* 308, no. 7 (2023): 2300033, https://doi.org/10.1002/mame.202300033.

37. X. Chen, L.-Q. Zou, J. Niu, W. Liu, S.-F. Peng, and C.-M. Liu, "The Stability, Sustained Release and Cellular Antioxidant Activity of Curcumin Nanoliposomes," *Molecules (Basel, Switzerland)* 20, no. 8 (2015): 14293–14311, https://doi.org/10.3390/molecules.

38. A. Tiwari, A. Singh, N. Garg, and J. K. Randhawa, "Curcumin Encapsulated Zeolitic Imidazolate Frameworks as Stimuli Responsive Drug Delivery System and Their Interaction With Biomimetic Environment," *Scientific Reports* 7, no. 1 (2017): 12598, https://doi.org/10.1038/s41598-017-12786-6.

39. Y. Zhang, Y. Jia, and L. Hou, "Synthesis of Zeolitic Imidazolate Framework-8 on Polyester fiber for PM2.5 Removal," *RSC Advances* 8, no. 55 (2018): 31471–31477.

40. R. Reshmi, K. R. Jiju, S. Suma, and A. S. Nair, "Folic Acid Grafted Aminated Zeolitic Imidazolate Framework (ZIF-8) as pH Responsive Drug Carrier for Targeted Delivery of Curcumin," *Journal of Drug Delivery Science and Technology* 79 (2023): 104098, https://doi.org/10.1016/j.jddst.2022.104098.

41. A. Ghaee, M. Karimi, M. Lotfi-Sarvestani, B. Sadatnia, and V. Hoseinpour, "Preparation of Hydrophilic Polycaprolactone/Modified ZIF-8 Nanofibers as a Wound Dressing Using Hydrophilic Surface

Modifying Macromolecules," *Materials Science and Engineering: C* 103 (2019): 109767, https://doi.org/10.1016/j.msec.2019.04.038.

42. N. G. Pillai, K. Archana, K. Y. Rhee, S.-J. Park, and A. Asif, "In Vitro Antiproliferative Study of Curcumin Loaded Nano Zeolitic Imidazolate Framework Hybrid Biomaterials on HeLa Cells," *Journal of Industrial and Engineering Chemistry* 79 (2019): 288–294, https://doi.org/10.1016/j.jiec.2019.06.023.

43. E. Guler, Y. E. Baripoglu, H. Alenezi, et al., "Vitamin D3/Vitamin K2/Magnesium-Loaded Polylactic Acid/Tricalcium Phosphate/Polycaprolactone Composite Nanofibers Demonstrated Osteoinductive Effect by Increasing Runx2 via Wnt/β-Catenin Pathway," *International Journal of Biological Macromolecules* 190 (2021): 244–258, https://doi.org/10.1016/j.ijbiomac.2021.08.187.

44. R. Babazade, E. Beyzanur Polat, B. Ertas, et al., "Synergistic Anticancer Effects of Metformin and *Achillea vermicularis* Trin-Loaded Nanofibers on Human Pancreatic Cancer Cell Line: An In Vitro Study," *European Polymer Journal* 179 (2022): 111565, https://doi.org/10.1016/j.eurpolymj.2022.111565.

45. Y. Shen and Y. Lv, "Dual Targeted Zeolitic Imidazolate Framework Nanoparticles for Treating Metastatic Breast Cancer and Inhibiting Bone Destruction," *Colloids and Surfaces B: Biointerfaces* 219 (2022): 112826, https://doi.org/10.1016/j.colsurfb.2022.112826.

46. H. Kaur, G. C. Mohanta, V. Gupta, D. Kukkar, and S. Tyagi, "Synthesis and Characterization of ZIF-8 Nanoparticles for Controlled Release of 6-Mercaptopurine Drug," *Journal of Drug Delivery Science and Technology* 41 (2017): 106–112, https://doi.org/10.1016/j.jddst.2017.04.002.

47. M. S. Monteiro, J. Lunz, P. J. Sebastião, and M. I. B. Tavares, "Evaluation of Nevirapine Release Kinetics From Polycaprolactone Hybrids," *Materials Sciences and Applications* 7, no. 11 (2016): 680–701, https://doi.org/10.4236/msa.2016.711060.

48. R. Li, Y. Song, P. Fouladian, et al., "Three-Dimensional Printing of Curcumin-Loaded Biodegradable and Flexible Scaffold for Intracranial Therapy of Glioblastoma Multiforme," *Pharmaceutics* 13, no. 4 (2021): 471, https://doi.org/10.3390/pharmaceutics13040471.

49. H. Jin, J. Pi, Y. Zhao, et al., "EGFR-Targeting PLGA-PEG Nanoparticles as a Curcumin Delivery System for Breast Cancer Therapy," *Nanoscale* 9, no. 42 (2017): 16365–16374, https://doi.org/10.1039/C7NR06898K.

50. E. Mosaffa, R. I. Patel, A. Banerjee, B. B. Basak, and M. Oroujzadeh, "Comprehensive Analysis of Cationic Dye Removal From Synthetic and Industrial Wastewater Using a Semi-Natural Curcumin Grafted Biochar/Poly Acrylic Acid Composite Hydrogel," *RSC Advances* 14, no. 11 (2024): 7745–7762, https://doi.org/10.1039/D3RA08521J.

51. Q. Zhang, D. Li, S. Guan, et al., "Tumor-Targeted Delivery of Honokiol via Polysialic Acid Modified Zein Nanoparticles Prevents Breast Cancer Progression and Metastasis," *International Journal of Biological Macromolecules* 203 (2022): 280–291, https://doi.org/10.1016/j.ijbiomac.2022.02.089.

52. M. Ajdary, M. A. Moosavi, M. Rahmati, et al., "Health Concerns of Various Nanoparticles: A Review of Their In Vitro and In Vivo Toxicity," *Nanomaterials* 8 (2018): 634, https://doi.org/10.20944/preprints201806.0273.v1.

53. J. Wu, Z. Zhang, J.g. Gu, et al., "Mechanism of a Long-Term Controlled Drug Release System Based on Simple Blended Electrospun Fibers," *Journal of Controlled Release* 320 (2020): 337–346, https://doi.org/10.1016/j.jconrel.2020.02.044.

54. M. Z. Fahmi, R. A. Prasetya, M. F. Dzikri, S. C. W. Sakti, B. Yuliarto, Irzaman, and Ferdiansjah, "$MnFe_2O_4$ nanoparticles/Cellulose Acetate Composite Nanofiber for Controllable Release of Naproxen," *Materials Chemistry and Physics* 250 (2020): 123055, https://doi.org/10.1016/j.matchemphys.2020.123055.

55. A. Q. Ansari, S. J. Ansari, M. Q. Khan, et al., "Electrospun Zein Nanofibers as Drug Carriers for Controlled Delivery of Levodopa in Parkinson Syndrome," *Materials Research Express* 6, no. 7 (2019): 075405, https://doi.org/10.1088/2053-1591/ab16bf.

56. Y. Xue, Z. Zhu, X. Zhang, et al., "Accelerated Bone Regeneration by MOF Modified Multifunctional Membranes Through Enhancement of Osteogenic and Angiogenic Performance," *Advanced Healthcare Materials* 10, no. 6 (2021), https://doi.org/10.1002/adhm.202001369.

57. Q. Wang, Y. Sun, S. Li, P. Zhang, and Q. Yao, "Synthesis and Modification of ZIF-8 and Its Application in Drug Delivery and Tumor Therapy," *RSC Advances* 10(62) (2020) 37600–37620, https://doi.org/10.1039/D0RA07950B.

58. B. R. Jermy, R. Y. Al-Jindan, V. Ravinayagam, and A. A. El-Badry, "Anti-Blastocystosis Activity of Antioxidant Coated ZIF-8 Combined With Mesoporous Silicas MCM-41 and KIT-6," *Scientific Reports* 12, no. 1 (2022): 6403, https://doi.org/10.1038/s41598-022-10397-4.

59. S. Yu, S. Wang, Z. Xie, et al., "Hyaluronic Acid Coating on the Surface of Curcumin-Loaded ZIF-8 Nanoparticles for Improved Breast Cancer Therapy: An In Vitro and In Vivo Study," *Colloids and Surfaces B: Biointerfaces* 203 (2021): 111759, https://doi.org/10.1016/j.colsurfb.2021.111759.

60. B. Farhood, K. Mortezaee, N. H. Goradel, et al., "Curcumin as an Anti-Inflammatory Agent: Implications to Radiotherapy and Chemotherapy," *Journal of Cellular Physiology* 234, no. 5 (2019): 5728–5740, https://doi.org/10.1002/jcp.27544.

61. M. Erkartal, U. Erkilic, B. Tam, et al., "From 2-Methylimidazole to 1,2,3-Triazole: A Topological Transformation of ZIF-8 and ZIF-67 by Post-Synthetic Modification," *Chemical Communications* 53, no. 12 (2017): 2028–2031, https://doi.org/10.1039/C6CC08746A.

62. M. Zheng, S. Liu, X. Guan, and Z. Xie, "One-Step Synthesis of Nanoscale Zeolitic Imidazolate Frameworks With High Curcumin Loading for Treatment of Cervical Cancer," *ACS Applied Materials & Interfaces* 7, no. 40 (2015): 22181–22187, https://doi.org/10.1021/acsami.5b07441.

63. S. Aydin, I. Kabaoglu, E. Guler, et al., "A Comparison Study of Fiber Diameter's Effect on Characteristic Features of Donepezil/Curcumin-Loaded Polycaprolactone/Polylactic Acid Nanofibers," *Macromolecular Materials and Engineering* 307, no. 5 (2022): 2100855, https://doi.org/10.1002/mame.202100855.

64. M. E. Cam, A. N. Hazar-Yavuz, S. Cesur, et al., "A Novel Treatment Strategy for Preterm Birth: Intra-Vaginal Progesterone-Loaded Fibrous Patches," *International Journal of Pharmaceutics* 588 (2020): 119782, https://doi.org/10.1016/j.ijpharm.2020.119782.

65. M. Abasalta, A. Asefnejad, M. T. Khorasani, and A. R. Saadatabadi, "Fabrication of Carboxymethyl Chitosan/Poly(ε-caprolactone)/Doxorubicin/Nickel Ferrite Core-Shell Fibers for Controlled Release of Doxorubicin Against Breast Cancer," *Carbohydrate Polymers* 257 (2021): 117631, https://doi.org/10.1016/j.carbpol.2021.117631.

66. M. A. Mohamady Hussein, E. Guler, E. Rayaman, et al., "Dual-Drug Delivery of Ag-Chitosan Nanoparticles and Phenytoin via Core-Shell PVA/PCL Electrospun Nanofibers," *Carbohydrate Polymers* 270 (2021): 118373, https://doi.org/10.1016/j.carbpol.2021.118373.

67. Q. Wu, M. Niu, X. Chen, et al., "Biocompatible and Biodegradable Zeolitic Imidazolate Framework/Polydopamine Nanocarriers for Dual Stimulus Triggered Tumor Thermo-Chemotherapy," *Biomaterials* 162 (2018): 132–143, https://doi.org/10.1016/j.biomaterials.2017.11.031.

68. A. M. Yilmaz Goler, A. Tarbin Jannuzzi, A. Biswas, et al., "Analysis of Quinolinequinone Analogs With Promising Cytotoxic Activity Against Breast Cancer," *Chemistry & Biodiversity* 20, no. 9 (2023): e202300848, https://doi.org/10.1002/cbdv.202300848.

Supporting Information

Additional supporting information can be found online in the Supporting Information section.

Supporting file 1: nano70048-sup-0001-SuppMat.docx